Inorganic Chemistry

Article

pubs.acs.org/IC

Probing Interligand Electron Transfer in the ^{1}MLCT S_1 Excited State of *trans*-$Mo_2L_2L'_2$ Compounds: A Comparative Study of Auxiliary Ligands and Solvents

Changcheng Jiang,*[,†] Philip J. Young,[‡] Samantha E. Brown-Xu,[§] William T. Kender,[†] Ewan J. M. Hamilton,[⊥] Judith C. Gallucci,[†] and Malcolm H. Chisholm[†]

[†]Department of Chemistry and Biochemistry, The Ohio State University, 100 West 18th Avenue, Columbus, Ohio 43210, United States

[‡]School of Chemistry, University of Nottingham, University Park, Nottingham NG7 2RD, U.K.

[§]Department of Chemistry, Northwestern University, Evanston, Illinois 60208, United States

[⊥]Department of Chemistry and Biochemistry, The Ohio State University at Lima, Lima, Ohio 45804, United States

Supporting Information

ABSTRACT: The interligand charge dynamics of the lowest singlet metal-to-ligand charge-transfer states (^{1}MLCT S_1 states) of a series of quadruply bonded *trans*-$Mo_2(NN)_2(O_2C{-}X)_2$ paddlewheel compounds are investigated, where NN is a π-accepting phenylpropiolamidinate ligand and $O_2C{-}X$ (X = Me, ^{t}Bu, T^{i}PB, or CF_3) is an auxiliary carboxylate ligand. The compounds show strong light absorption in the visible region due to MLCT transitions from the Mo_2 center to the NN ligands. The transferred electron density was followed by femtosecond time-resolved infrared (fs-TRIR) spectroscopy with vibrational reporters such as the ethynyl groups on the NN ligands. The observed fs-TRIR spectra show that these compounds have asymmetric ^{1}MLCT S_1 excited states where the transferred electron mainly resides on a single NN ligand. The presence of interligand electron transfer (ILET) is suggested to explain the shape of the ν(C≡C) bands and the influence of auxiliary ligands and solvents on the interligand electronic coupling. The ILET in the ^{1}MLCT S_1 state is shown to be sensitive to the functional groups on the auxiliary ligands while being less responsive to changes in solvents.

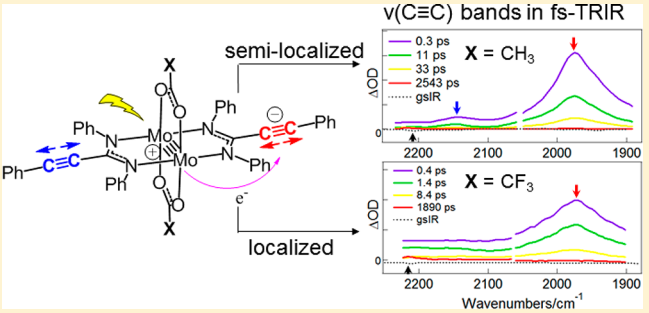

INTRODUCTION

The photophysics of transition metal (TM) complexes present an opportunity for the application of fundamental research in inorganic chemistry.[1−3] TM complexes with high-energy and long-living charge-transfer excited states have found wide applications in the area of solar energy conversion and photocatalysis.[4,5] However, some fundamental questions on the nature of the excited-state charge dynamics of TM complexes remain, such as a clear description of the charge distribution in compounds with equivalent ligands or metal centers.[1,6,7] The location of the positive or negative charge in such charge-transfer excited states can be difficult to assign. A simple description using integer point charges can be insufficient or inaccurate when considering electron transfer and other interactions between the identical redox centers. In previous works, the charge distribution in charge-transfer exited states of TM compounds has been studied by spectroscopic methods such as luminescence, Stark spectroscopy, and transient absorption spectroscopy as well as by computational studies.[8−10] In recent years, femtosecond time-resolved infrared (fs-TRIR) spectroscopy has become a more reliable and direct method to study excited-state photophysics.

In the Chisholm group, we have focused on the lowest metal-to-ligand charge-transfer singlet states (^{1}MLCT S_1 states) of *trans*-$M_2L_2L'_2$ and M_2L_4 paddlewheel compounds (M = Mo or W) containing metal−metal quadruple bonds and π-accepting ligands. The MLCT states of these d^4−d^4 metal dimers were shown to display a variety of charge-distribution patterns with respect to the transferred electron.[11−14] The distribution of the electron ranges from being totally localized, semilocalized, and totally delocalized over the acceptor ligands. For example, the transferred electron was found to be localized on one $(NPh)_2CC{\equiv}CPh$ ligand in the ^{1}MLCT S_1 state of $Mo_2[(NPh)_2CC{\equiv}CPh]_4$,[15] whereas it was found to be semilocalized over two $(N^iPr)_2CC{\equiv}CPh$ ligands in the ^{1}MLCT S_1 state of *trans*-$Mo_2[(N^iPr)_2CC{\equiv}CPh]_2(O_2CMe)_2$ and fully delocalized over two $(NPh)C(S)C{\equiv}CPh$ ligands in

Received: May 8, 2017

DOI: 10.1021/acs.inorgchem.7b01164
Inorg. Chem. XXXX, XXX, XXX−XXX

the ^{1}MLCT S_1 state of *trans*-$Mo_2[(NPh)C(S)C{\equiv}CPh]_2(O_2C{-}T^iPB)_2$.[11,16]

We have previously suggested that the observed charge-distribution patterns in the ^{1}MLCT S_1 states of *trans*-$M_2L_2L'_2$ and M_2L_4 compounds are the results of an interligand electron transfer (ILET) process on the vibrational time scale (~10^{-12} s), where "fast" ILET is associated with MLCT states delocalized over multiple ligands, while "slow" ILET is associated with MLCT states localized on one ligand.[16] Due to the mediator role of the dimetal center, the electron transfer can be greatly influenced by the electronic properties of the bimetallic core and its interactions with the acceptor ligands.[12,16]

Here, a series of *trans*-$Mo_2L_2L'_2$ amidinate compounds (shown in Figure 1) were prepared with different carboxylate

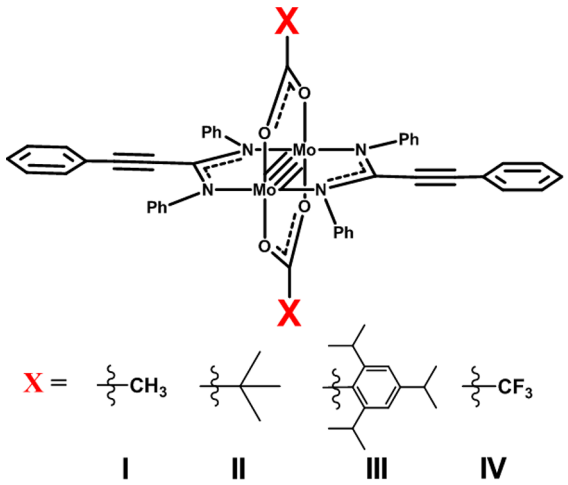

Figure 1. General structure of **I**–**IV**.

auxiliary ligands, namely, *trans*-$Mo_2(NN)_2(O_2C\text{-}Me)_2$ (**I**), *trans*-$Mo_2(NN)_2(O_2C\text{-}^tBu)_2$ (**II**), *trans*-$Mo_2(NN)_2(O_2C\text{-}T^iPB)_2$ (**III**), and *trans*-$Mo_2(NN)_2(O_2C{-}CF_3)_2$ (**IV**), where NN = *N,N′*-diphenylphenylpropiolamidinate, and Me = methyl, ^{t}Bu = *tert*-butyl, T^iPB = 2,4,6-triisopropylbenzyl, and CF_3 = trifluoromethyl. Preparation and characterization of compound **III** were reported previously.[15] These compounds show strong MLCT transitions to the NN ligands but not the carboxylate ligands.

The excited-state photophysics of **I**–**IV** and the interligand charge dynamics between NN ligands were examined with respect to perturbations exerted by the auxiliary carboxylate ligands. Considering previous reports of charge localization in these compounds (the dipole moment of the excited states is a function of electron localization), the influence of solvent dipoles on the charge distribution was also investigated.[11,15]

RESULTS AND DISCUSSION

Synthesis and Crystal Structure. Compounds **I**–**IV** were prepared using a common synthetic method where two equivalents of the NN ligand (lithium *N,N′*-diphenylphenylpropiolamidinate) were reacted with one equivalent of the appropriate Mo_2L_4 carboxylate compound.[17−19] The compounds were purified through solution processes, and the purity of each was confirmed by NMR and MALDI-TOF mass spectrometry. The structures of **I**–**IV** obtained by single-crystal X-ray crystallography are displayed in Figure 2.

The core structures of **I**–**IV** have effective D_{2h} symmetry. All of the molecules adopt the *trans* configuration, in which the plane of the carboxylate ligands is perpendicular to the plane of the NN ligands. Those on the NN ligands in **I**–**IV** are found to be coplanar with the $CN_2{-}Mo_2{-}N_2C$ plane. The phenylacetylenyl groups in **III** are slightly tilted due to the arrangement of the phenyl groups on the nitrogen atoms. All of the phenyl groups on the donor nitrogen atoms are effectively twisted (~50−80°) away from the CN_2 plane.

All four compounds display Mo−Mo bond lengths of around 2.10 Å, typical of Mo−Mo quadruple bonds,[20] and average Mo−N and Mo−O bond lengths of around 2.13 and 2.12 Å, respectively. The Mo−Mo and Mo−O bond lengths in **IV** are slightly longer (by ~0.02 Å) than those in **I**–**III**, likely due to the influence of the strongly electron-withdrawing $-CF_3$

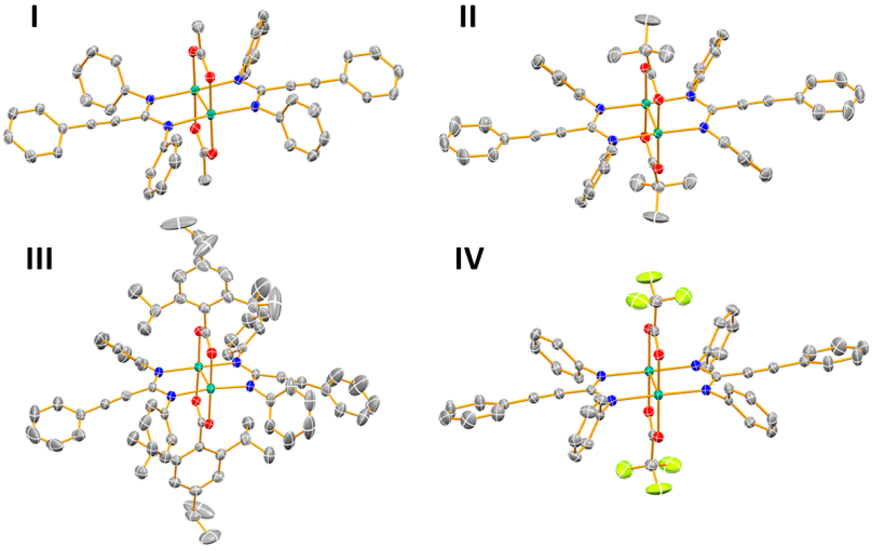

Figure 2. Crystal structures of **I**–**IV** with thermal ellipsoids drawn at the 50% probability level. Hydrogens and solvent molecules were omitted for clarity. Green = molybdenum, blue = nitrogen, red = oxygen, gray = carbon, and yellow = fluorine. (The plot of **III** was adapted from ref 15 with permission from American Chemical Society.)

DOI: 10.1021/acs.inorgchem.7b01164
Inorg. Chem. XXXX, XXX, XXX−XXX

groups.[21] The intramolecular distance between the C≡C bond centers is around 9.7 Å in **I**–**IV**.

In the solid-state, each Mo center in **II** and **IV** was found to be coordinated by a dimethyl sulfoxide (DMSO) solvent molecule, while only one metal in **I** and **III** was so coordinated. The crystal structures of **I**–**IV** including coordinating solvent molecules are displayed in Figures S9 and S10 in the Supporting Information.

Ground-State Infrared Spectroscopy. The C≡C bonds, phenyl rings, and CN_2 moieties on the NN ligands and CO_2 moieties on the carboxylate ligands are convenient IR reporter groups for the excited-state charge distribution and interligand charge dynamics. **I**–**IV** were studied in solution by FT-IR spectra to identify their signature vibrational bands. The IR spectra of **I**–**IV** in tetrahydrofuran (THF) are shown in Figure 3, and the IR spectra of **III** in toluene, dichloromethane

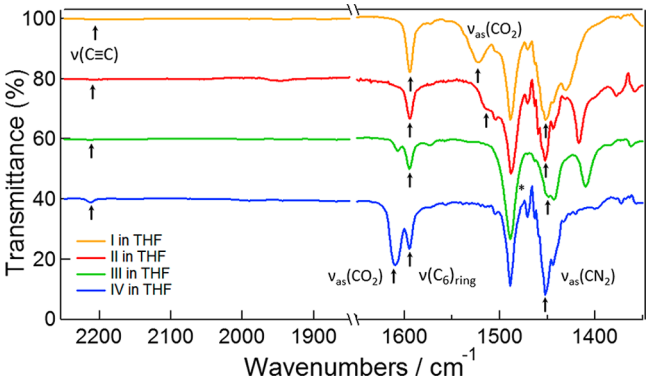

Figure 3. FT-IR spectra of **I**–**IV** in THF solution. The spectra lines are plotted with an offset from each other on the *Y* axis. *The $\nu_{as}(CO_2)$ of **III** was masked.

(DCM), and dimethylformamide (DMF) are shown in Figure S11 in the Supporting Information. Frequency calculations were used to assist the assignments of above-mentioned vibrational bands. The calculated IR spectra of **I**–**IV** are shown in Figure S12 in the Supporting Information.

The vibrational bands belonging to the NN ligands appear at similar frequencies in the ground states of **I**–**IV**. A weak band at around 2210 cm^{-1} was found for the ν(C≡C) stretch; two sharp bands, one at around 1595 cm^{-1} and one at around 1490 cm^{-1}, were found for $\nu(C_6)_{ring}$ stretches of two different modes, and a strong band at around 1450 cm^{-1} was found for the asymmetric $\nu(CN_2)$ stretch. The irregular shape of the $\nu(CN_2)$ bands is due to strong solvent absorption in the region. The weaker, neighboring bands at 1605 and 1480 cm^{-1} in **III** were attributed to the $\nu(C_6)_{ring}$ stretching bands in the $-T^iPB$ moiety.

In comparison, the asymmetric $\nu(CO_2)$ stretching bands of **I**–**IV** appear over a wider range of frequencies due to different functional groups. A strong $\nu(CO_2)$ band was found at 1523 cm^{-1} for **I**, at 1515 cm^{-1} for **II**, and at 1623 cm^{-1} for **IV**. The $\nu(CO_2)$ band for **III** likely occurs near 1490 cm^{-1} (as spotted in the ground-state bleach in the fs-TRIR spectra of **III**), where it is masked by the strong $\nu(C_6)_{ring}$ band.[15] The high energy of the $\nu(CO_2)$ vibrations in **IV**, again, is a result of the electron-withdrawing nature of the $-CF_3$ groups which depopulated the electron density in the π^* orbital of the carboxylate ligand.

Compound **III** in solvents of differing polarities was also studied by FT-IR spectroscopy, as shown in Figure S11. The frequencies of the ν(C≡C) and $\nu(C_6)_{ring}$ bands did not shift significantly with respect to change of solvents. The $\nu(CN_2)$ bands, alternatively, shifted slightly to a higher energy from the toluene to DCM to THF solutions.

Electronic Absorption and Emission Spectroscopy. Compounds **I**–**IV** display intense absorption and weak fluorescence emission in solution at room temperature. The UV–vis absorption and emission spectra of **I**–**IV** collected in THF are shown in Figure 4A, and the spectra of **III** in toluene,

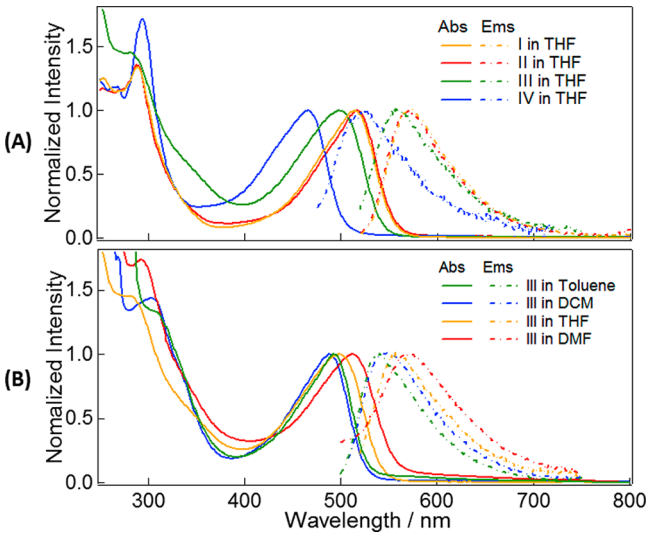

Figure 4. Normalized absorption (Abs) and emission (Ems) spectra of **I**–**IV**, (A) **I**–**IV** in THF solution and (B) **III** in toluene, DCM, THF, and DMF solutions.

DCM, THF, and DMF are shown in Figure 4B. Quantitative parameters like the MLCT maxima, molar extinction coefficients (ε), and fluorescence quantum yields (Φ_{FL}) are summarized in Table 1.

As shown by Figure 4 and Table 1, the MLCT transitions of **I**–**IV** were significantly influenced by both the carboxylate ligands and the solvents. In THF, **II** featuring the *tert*-butylcarboxylate ligands shows the lowest-energy MLCT band at 517 nm, and **IV** featuring the trifluoroacetate ligands shows the highest-energy MLCT band at 486 nm, with an energy difference of ~1240 cm^{-1}. The molar extinction coefficient of **II** is almost double that of **IV**.

With respect to solvent environments, **III** shows the lowest-energy MLCT absorption in DMF and the highest-energy MLCT absorption in DCM (not toluene). DMF significantly broadens the MLCT band and shifts it by ~980 cm^{-1}. The observed solvatochromism here is in accordance with strong dipole–dipole interactions, as well as factors like solvent coordination (Figure S9 and S10) and also π–π stacking interactions.

The emission spectra of **I**–**IV** in the visible range are all identified as fluorescence from the ^{1}MLCT S_1 states. The quantum yields are generally well-below 1% due to charge-transfer transitions and strong competition from intersystem crossing. The fluorescence bands of **I**–**IV** resemble the MLCT absorption bands with respect to both their shapes and trends in energy. These compounds also show strong phosphorescence from the lowest metal-centered triplet states ($^3\delta\delta^*$ T_1 states) in the near-infrared region (~800–1100 nm), but they are not discussed here as they are outside the scope of this

DOI: 10.1021/acs.inorgchem.7b01164
Inorg. Chem. XXXX, XXX, XXX–XXX

Table 1. Photophysical Data of I–IV for the MLCT Transitions

compounds	solvent	absorption λ_{max}/nm	ε/M^{-1}cm^{-1}	fluorescence λ_{max}/nm	Φ_{FL}/%	Stokes shift/cm^{-1}
I	THF	514	37 600	573	0.20	2000
II	THF	517	41 600	570	0.23	1800
III	toluene	494	29 900	541	0.13	1800
	DCM	489	33 000	545	0.09	2100
	THF	498	29 400	557	0.19	2360
	DMF	514	24 600	571	0.17	1940
IV	THF	466	23 900	525	0.03	2410

paper. The Stokes shifts, which measure the energy difference between the vertical absorption and emission transitions, range from 1800 and 2410 cm^{-1} for **I–IV**. **IV** shows the largest Stokes shift and lowest fluorescence quantum yield.

Femtosecond Time-Resolved Infrared Spectroscopy. The ^{1}MLCT S_1 states of **I–IV** were further studied using femtosecond time-resolved infrared (fs-TRIR) spectroscopy. The spectra display vibrational bands that are present in the ^{1}MLCT S_1 state and the $^3\delta\delta^*$ T_1 state, as seen for similar compounds.[11,22,15,16] The shifts in the vibrations, whether to higher or lower energy from the ground state, provide information on the charge-density distribution and charge dynamics in the excited states.

The S_1 lifetimes of **I–IV** found in the fs-TRIR spectra are between 10 and 21 ps, as shown in Table 2. The kinetic traces

Table 2. ^{1}MLCT S_1 State Lifetimes of Compounds I–IV

compounds	solvents	$\tau(S_1)$/ps
I	THF	19.0 ± 0.4
II	THF	21.4 ± 0.9
III	toluene	15.5 ± 0.3
	THF	19.1 ± 0.4
	DMF	15.2 ± 0.9
IV	THF	10.5 ± 2.3

and exponential fitting plots of **I–IV** are displayed in S14 and 15. In all cases, a short lifetime component (<1 ps) and a longer lifetime component were found for the ^{1}MLCT S_1 state features, where the former was attributed to intramolecular relaxation processes.

fs-TRIR Spectra of I–IV in THF Solution. The fs-TRIR spectra of **I–IV** were collected in THF solution at room temperature with excitation of **I–IV** into their MLCT bands, **I–III** at 515 nm, and **IV** at 400 nm. The fs-TRIR spectra of **I–IV** in the range of 1350–2250 cm^{-1} with selected time delays are shown in Figure 5. For each compound, the inverted ground-state IR spectrum is also plotted as a dotted line for reference.

The fs-TRIR spectra of **I–IV** at early time delays (purple and blue traces) are associated with the ^{1}MLCT S_1 states. Strong absorption bands of the ν(C≡C) and $\nu(C_6)_{ring}$ stretches were observed; these stretches show significant shifts to lower wavenumbers compared to the ground state, in accordance to the displacement of electron density from the Mo_2 center to the π^* antibonding orbitals of the NN ligands.

In the ^{1}MLCT S_1 states of **I–III**, each compound displays two transient ν(C≡C) features, a strong absorption band at ~1970 cm^{-1} and a weak absorption band at ~2150 cm^{-1}. The two ν(C≡C) stretches are shifted by −235 and −65 cm^{-1} in **I**, −230 and −64 cm^{-1} in **II**, and −230 and −70 cm^{-1} in **III**. Each compound also shows one $\nu(C_6)_{ring}$ absorption band at ~1560

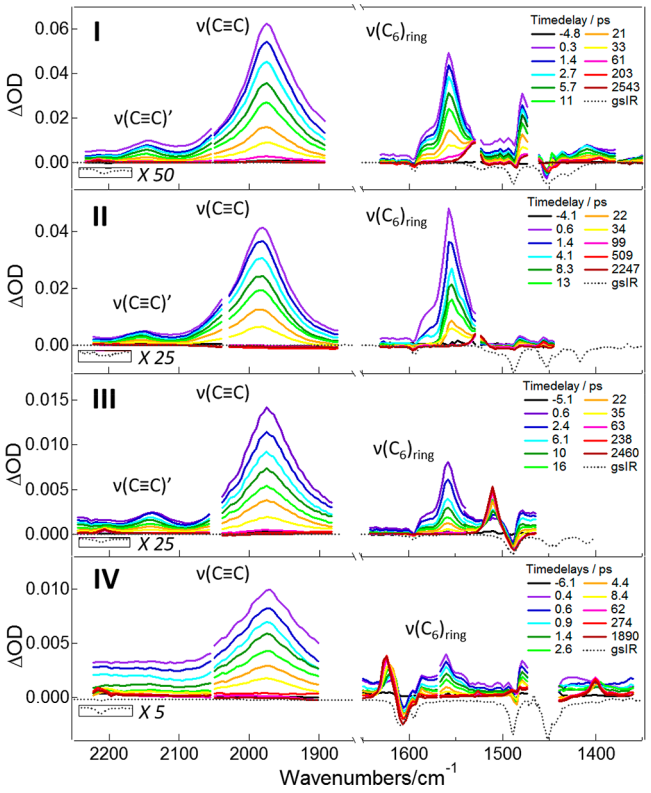

Figure 5. fs-TRIR spectra of **I–IV** in THF solution at room temperature with inset showing time delays. Inverted ground-state IR (gs-IR) spectra are shown by dotted lines.

cm^{-1} together with a ground-state bleach band at ~1595 cm^{-1}. The $\nu(C_6)_{ring}$ stretches are shifted around −40 cm^{-1}. The observation of two ν(C≡C) bands in **I–III**, as suggested in previous works, corresponds to two unequally reduced NN ligands in the ^{1}MLCT S_1 state.[11,15,16]

The fs-TRIR spectra of **IV**, however, are quite different. The most noticeable feature is that only one ν(C≡C) transient feature was observed at picosecond time delays. The strong ν(C≡C) band of **IV** is observed at 1970 cm^{-1}, with a shift of −230 cm^{-1}. This ν(C≡C) band (fwhm ≈ 120 cm^{-1}) is much broader compared to those of the other three compounds (fwhm ≈ 90 cm^{-1}). The expected weaker ν(C≡C) band, however, was missing or too weak to be detected. This presence of a single ν(C≡C) band that is ~230 cm^{-1} shifted indicates that only one NN ligand was reduced in the ^{1}MLCT S_1 state of **IV**.

In tens of picoseconds, both the ν(C≡C) and the $\nu(C_6)_{ring}$ bands of the ^{1}MLCT S_1 states decay away and features corresponding to the $\nu(CO_2)$ and $\nu(CN_2)$ stretches of the $^3\delta\delta^*$ T_1 states emerge (red traces). Most apparent are the asymmetric $\nu(CO_2)$ vibrations which shift ~15 cm^{-1} to higher

DOI: 10.1021/acs.inorgchem.7b01164
Inorg. Chem. XXXX, XXX, XXX–XXX

energy from the ground state (due to reduced back-bonding donation to the π^* orbital from the $Mo_2\delta$ bond). A weak $\nu(C{\equiv}C)$ absorption band was also observed at ~2200 cm^{-1} in each of **I**–**IV**, close to the ground-state frequency. No $\nu(C_6)_{ring}$ bands were spotted in the $^3\delta\delta^*$ T_1 state. These spectral changes clearly depict the ^{1}MLCT $S_1 \rightarrow {}^3\delta\delta^*$ T_1 intersystem crossing process, in which the electron transfers back from the NN ligands to the Mo_2 center.

fs-TRIR Spectra of ***III*** *in Solvents of Different Polarities.* In addition to THF at room temperature, the excited states of **III** were examined in toluene, DCM, and DMF solution to study the solvent influence. The spectra of **III** in toluene, THF, and DMF are shown in Figure 6. The DCM solution yielded no useable spectra, presumably due to photochemical decomposition. The fs-TRIR spectra of **III** in DMF solution were not collected in the 1400–1500 cm^{-1} region due to strong solvent absorption.

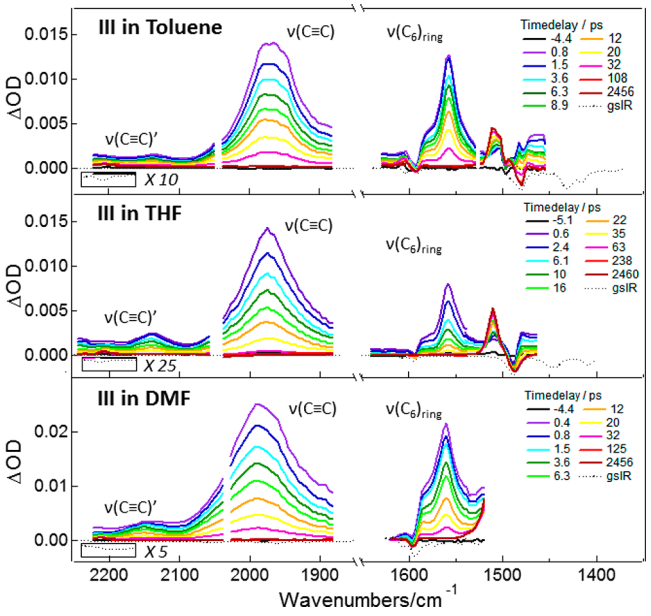

Figure 6. fs-TRIR spectra of **III** in toluene, THF, and DMF solution with inset showing time delays. Inverted ground-state IR (gs-IR) spectra are shown by dotted lines.

We have previously established that the ^{1}MLCT S_1 state of **III** is not symmetrical and that there should be a significant dipole moment associated with the excited state species.[15] That means, strong dipole–dipole interactions between the ^{1}MLCT S_1 state of **III** and the solvent molecules are expected. Interestingly, similar to the fs-TRIR spectra of **III** in THF, two $\nu(C{\equiv}C)$ bands (one weak, one strong) were observed for the ^{1}MLCT S_1 state of **III** in toluene and DMF. The $\nu(C{\equiv}C)$ bands are shifted by −75 and −240 cm^{-1} in toluene and by −60 and −220 cm^{-1} in DMF, which are quite similar compared to shifts of −70 and −235 cm^{-1} in THF.

The ^{1}MLCT S_1 lifetime of **III** is 15.5 ps in toluene and 15.2 ps in DMF. The band shapes and early ^{1}MLCT kinetics in toluene, THF, and DMF are different according to Figure 6 and the exponential fitting shown in Figure S15. However, the electron-density distribution in the ^{1}MLCT S_1 state of **III** are qualitatively the same in all three solvents. The shifts in DMF solution are smaller than those of the other two solutions, which is surprising given that a polar solvent is expected to stabilize charge-transfer states.

Density Functional Theory Calculations. The electronic structures and electronic transitions of **I**–**IV** were investigated by density functional theory (DFT) and time-dependent density functional theory (TD-DFT) methods, respectively, using the B3LYP functional and the Gaussian 09 suite.[23,24]

The frontier molecular orbital (MO) energy diagram and MO surface plots of **I**–**IV** in the gas phase are shown in Figure 7.

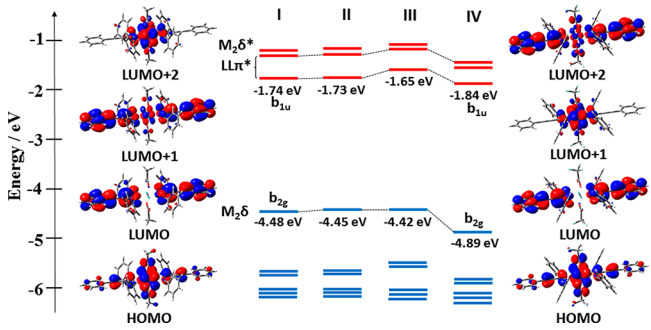

Figure 7. MO energy levels and orbital surface plots of **I**–**IV**. LUMO +2, LUMO+1, LUMO, and HOMO are shown for **I** (left) and **IV** (right), respectively.

The electronic structures of Mo_2 paddlewheel compounds are best described by interactions between the Mo_2 quadruple bond orbitals and combinations of the ligand π^* orbitals.[12] With the NN ligands in the *trans* orientation, there are two possible NN π^* orbital combinations: the in-phase combination which does not interact with the $Mo_2\delta$ bond orbital and the out-of-phase combination which does.

As shown in Figure 7, the highest occupied molecular orbital (HOMO, b_{2g}) of **I**–**IV** is mainly composed of the $Mo_2\delta$ orbital and the out-of-phase LLπ^* orbital of the NN ligands. The lowest unoccupied molecular orbital (LUMO, b_{1u}) of **I**–**IV** is mainly made up of the in-phase LLπ^* orbital of the NN ligands. The HOMOs and LUMOs of **I**–**IV** appear rather similar except for the energy level difference. No significant contribution from the metal center or the carboxylate ligands was observed in the LUMO.

In compound **IV**, the $Mo_2\delta$-based HOMO is lower in energy by ~0.4 eV compared to those of **I**–**III**, which is attributed to the strong electron-withdrawing ability of the $-CF_3$ groups. A similar effect is seen on the $Mo_2\delta^*$-based orbital, which moves lower than the out-of-phase NN LLπ^* orbital. In compound **III**, the LLπ^*-based LUMO is higher in energy by 0.1 eV than those of **I** and **II**, which is attributed to steric influences of the $-T^iPB$ groups over the NN ligands. The lower HOMO in **IV** and the higher LUMO in **III** lead to the increased energies of the MLCT transitions compared to **I** and **II**.

Time-dependent density functional theory (TD-DFT) calculations were used to examine the electronic transitions of **I**–**IV**. The results show that the MLCT transitions of **I**–**IV** can be described fully as HOMO to LUMO transitions. This is convenient since we can look at the composition of the LUMO for information on the excited-state electron population. The lowest two transitions of **I**–**IV** in the visible range are described in Table 3.

As shown in Table 3, the MLCT transitions of **I**–**IV** are predicted to be fully allowed transitions. The predicted energies

DOI: 10.1021/acs.inorgchem.7b01164
Inorg. Chem. XXXX, XXX, XXX–XXX

Table 3. Electronic Transitions in I–IV As Predicted by TD-DFT[a]

compounds	transition	origin	λ/nm	f
I	$S_0 \rightarrow S_1$	HOMO → LUMO	530	1.0329
	$S_0 \rightarrow S_2$	HOMO → 0.92 LUMO+2 (δ^*)	493	0.0003
II	$S_0 \rightarrow S_1$	HOMO → LUMO	534	1.0050
	$S_0 \rightarrow S_2$	HOMO → 0.92 LUMO+2 (δ^*)	492	0.0002
III	$S_0 \rightarrow S_1$	HOMO → LUMO	528	0.8746
	$S_0 \rightarrow S_2$	HOMO → 0.92 LUMO+2 (δ^*)	496	0.0002
IV	$S_0 \rightarrow S_1$	HOMO → 0.91 LUMO+1 (δ^*)	489	0.0005
	$S_0 \rightarrow S_2$	HOMO → LUMO	475	1.0268

[a] λ is the transition wavelength and f is the oscillator strength.

match reasonably well with those observed in absorption spectra. It is interesting that the MLCT transitions of **I–III** are predicted as $S_0 \rightarrow S_1$ transitions, but the MLCT transition in **IV** is a $S_0 \rightarrow S_2$ transition where it surpasses the energy of the $\delta \rightarrow \delta^*$ transition. However, according to the emission spectra and the fs-TRIR spectra, the S_1 states of **I–IV** are all indeed ^{1}MLCT in nature. No features of a $^1\delta\delta^*$ S_1 state were observed, and these often have signature lifetimes of ~50 ps.[25]

The composition of the frontier MOs in **I–IV** was studied by natural bonding orbital (NBO) analysis.[26,27] Due to the property differences between the metal orbitals and the ligand orbitals, they are often differentiated from each other. The percentage contributions of the metal orbitals are summarized in Table 4.

Table 4. Metal-Orbital Contribution (%) to the Frontier MOs in I–IV

compounds	HOMO	LUMO	LUMO+1	LUMO+2
I	65.2	1.2	6.5	76.8
II	65.1	1.1	6.6	76.7
III	64.6	1.3	6.0	76.9
IV	62.9	1.3	76.7	3.9

The composition of the HOMO and LUMO provide approximate descriptions of the electron-density distribution in the ground state and upon transitioning to the ^{1}MLCT state. As shown in Table 4, molybdenum orbitals and the NN ligand orbitals contribute consistently to the HOMO of **I–IV,** where the metal accounts for over 60% of the to the HOMO. The NN ligand contributions remain effectively the same despite changes in the carboxylate ligands.

As for the LUMO, the NN ligand orbitals contribute almost exclusively to the LUMO of **I–IV** while the metal orbitals contribute less than 1.5%, consistently. The trivial metal-orbital contributions to the LUMO of **I–IV** are mainly of $Mo_2\pi_{5p}$ character, which is in strong contrast to the previously studied *trans*-$Mo_2L_2L'_2$ compound with (NPh)C(O)C≡CPh and (NPh)C(S)C≡CPh ligands. The latter displayed significant $Mo_2\delta^*_{4d}$ contribution (~3.4% and ~10%) to the LUMO.[15,16] The limited metal-orbital contribution indicates that interligand electronic interactions can be rather weak in their MLCT states as there is no direct orbital contact.

DISCUSSION

Using a donor–acceptor (D–A) description, *trans*-$Mo_2L_2L'_2$ compounds **I–IV** can be viewed as A–D–A type compounds. When the transferred electron is equally shared by the two acceptor ligands in the MLCT state (i.e., $A^{-1/2}$–D^+–$A^{-1/2}$), only one IR-active ν(C≡C) stretch is expected since the excited state is still symmetrical.[16] When the transferred electron is totally localized on one acceptor ligand (i.e., A^-–D^+–A), two IR-active ν(C≡C) stretches are expected but only one would be shifted from the ground-state wavenumber value.[16] In the intermediate case where the transferred electron is unequally shared (i.e., $A^{-(1-\alpha)}$–D^+–$A^{-\alpha}$), two discrete ν(C≡C) bands are expected, both of which are shifted from the ground state.[16] The last scenario, which leads to an asymmetrical, semidelocalized excited state, has been studied before. In a paper from 2006, Terenziani et al. formulated the quantum mechanics of charge-transfer states in organic A–D–A and D–A–D type molecules and predicted unequal charge separation under certain circumstances.[28]

In inorganic chemistry, classic mixed valence (MV) compounds offer convenient precedents for dealing with unequal oxidation numbers and open-shell electronic structures of symmetrical molecular systems.[29] The Robin–Day scheme, which is frequently used to describe charge localization/delocalization in the ground state of MV complexes, can be adapted here to describe the electron-density distribution in the ^{1}MLCT excited states. In the same spirit, a class I ^{1}MLCT state corresponds to a transferred electron totally localized on one ligand, a class III ^{1}MLCT state to a transferred electron totally delocalized over two or more ligands, and a class II ^{1}MLCT state to the intermediate case. In analogy to intramolecular electron transfer in MV compounds, interligand electron transfer (ILET) can be used elegantly to describe interligand interactions in these MLCT excited states.

The observed shifts of the ν(C≡C) bands in the ^{1}MLCT S_1 states of **I–IV** are summarized in Table 5. The electron delocalization over the ligands in ^{1}MLCT S_1 states are assigned with MV classifications as we described.

Table 5. Shifts of ν(C≡C) Bands and MV Assignments of the ^{1}MLCT S_1 States of I–IV

compounds	solvent	ν(C≡C) shift in S_1 state/cm^{-1}	MV classification
I	THF	−65, −235	class II
II	THF	−64, −230	class II
III	toluene	−75, −240	class II
	THF	−70, −235	class II
	DMF	−60, −220	class II
IV	THF	−230	class I

The ^{1}MLCT S_1 states of **I–III** were assigned as class II based on the two ν(C≡C) bands observed in their fs-TRIR spectra, which suggests that the transferred electron is semilocalized between the two NN ligands. In **IV**, the single observed ν(C≡C) band suggests that the ^{1}MLCT S_1 state is a class I type, and the electron density is present exclusively on one of the two NN ligands. We have previously studied the fs-TRIR spectra of $(DAniF)_3Mo_2(O_2CC{\equiv}CPh)$,[30] which is a similar compound functionalized with a single MLCT ligand, and the transferred electron is necessarily localized. A single ν(C≡C) band was observed in the ^{1}MLCT S_1 state with a shift of 240 cm^{-1}, which agrees well with the fs-TRIR spectra of **IV**.

The surrounding solvent molecules appear to have limited influence on the mixed valence phenomena in the MLCT excited states. The ^{1}MLCT S_1 states of **III** in the nonpolar toluene and the polar DMF solutions are both showing similar ν(C≡C) band structures, as in THF. The coordinating and

DOI: 10.1021/acs.inorgchem.7b01164
Inorg. Chem. XXXX, XXX, XXX–XXX

close-contacting solvent molecules still strongly influence the excited-state relaxation as we see from the fluorescence quantum yields and relaxation dynamics. Yet the interligand interactions were hardly affected. With classic MV complexes, numerous studies have been conducted on the influence of solvents on electron transfer in the ground state of class II and III "borderline" compounds.[29,31] However, few simple and widely accepted conclusions were reached.

The conditions for localized and delocalized electron transfer in these excited-state mixed valence systems are not clear yet, and possibly involve multiple determining factors that control the interligand coupling. On the basis of our results, the metal−ligand orbital mixing in the frontier orbitals appears to be essential. $Mo_2\delta^*$ contribution to the single-occupied LUMO in the ^{1}MLCT S_1 states of the paddlewheel compounds, in particular, contributes to the strong interligand interactions.[16] The localized character of the ^{1}MLCT S_1 states of **I**−**IV** is consistent with very limited contribution of the $Mo_2\delta^*$ orbital in their LUMO.

The more localized character of the ^{1}MLCT S_1 state of **IV** is intriguing compared to the other three. The DFT investigations on the ground states of **I**−**IV** fall short to reveal significant factors that would contribute to different long-range interligand interactions. Excited-state calculations of large TM complexes have not yet been efficient and reliable and thus were not employed in this study.

Since the influence on the mixed valence of **I**−**IV** comes from the functional groups on the O_2C−X ligands, the localization could be because of Coulombic interactions related to their electron-donating or electron-withdrawing abilities. The cross configuration of the auxiliary ligands and the MLCT ligands makes it tempting to compare the structure of compounds **I**−**IV** to that of a field-effect transistor (FET). It is possible that the ILET in *trans*-$Mo_2L_2L'_2$ compounds can be modulated just like a FET by Coulombic interactions through changing the "gate" potentials.

Due to the ultrashort lifetimes of the charge-transfer S_1 states of TM complexes, charge-distribution patterns in the ^{1}MLCT states of TM complexes have only been studied in a few systems (for example, $Ru(bpy)_3^{2+}$, $Fe(bpy)_3^{2+}$, and $Re(bpy)(CO)_3Cl$).[32−34] There have been reports on interligand interactions in the ^{3}MLCT T_1 states of TM complexes that have much longer lifetimes, such as *trans* Pt(II) bis-acetylides and Re(I) heteroleptic polypyridine complexes.[35,36] The Pt(II) bis-acetylides bear similarities to the compounds studied here, and the current literature appears to favor the idea that the ^{1}MLCT/^{1}LLCT excited states of these compounds are delocalized while the ^{3}MLCT/^{3}LLCT excited states are localized.[8,37,38]

Dereka et al. recently reported a fs-TRIR study of the charge-transfer S_1 state ($\tau \approx 1$ ns) of a bis-cyanophenyl pyrrolopyrrole, an A−D−A type organic compound having two terminal C≡N reporter groups.[39] The charge-distribution pattern in its S_1 state showed strong solvent dependence, where it displayed a single shifted ν(C≡N) band in nonpolar solvents (assigned to a delocalized S_1 state) and two unequal ν(C≡N) bands in polar solvents (assigned to an asymmetrical, localized S_1 state). While the same solvent dependence was not observed, the resemblance between the dual ν(C≡N) bands observed in this A−D−A type organic compound and the dual ν(C≡C) bands observed in **I**−**III** is remarkable.

Finally, the real-time symmetry breaking from the presumably delocalized Franck−Condon states of compounds **I**−**IV** was not directly observed. The ^{1}MLCT S_1 states of **I**−**IV** are already asymmetrical by ∼200 fs according to the fs-TRIR spectra, which is the time resolution of our instrument.

CONCLUSION

The excited-state photophysics of the ^{1}MLCT S_1 states of a series of *trans*-$Mo_2(NN)_2(O_2C-X)_2$ paddlewheel compounds were examined in solution at room temperature. The transferred electron from the dimetal center to the accepting ligands was followed with ν(C≡C) stretches located on the ligands using fs-TRIR spectroscopy. Although having two equivalent NN ligands, the ^{1}MLCT S_1 states of these compounds are not symmetrical, and the transferred electron is shared unequally over the NN ligands.

The auxiliary carboxylate ligands O_2C−X displayed significant influences over the interligand interactions between the NN ligands. The observed ν(C≡C) patterns are explained in the construct of excited-state mixed valence in an A−D−A type donor−acceptor system. An interligand electron transfer (ILET) process is suggested to exist in the ^{1}MLCT S_1 states of these compounds, which are modulated by the auxiliary ligands. DFT studies have shown evidence of the involvement of metal orbitals in the interligand electronic coupling.

The demonstration of control over excited-state charge dynamics through the choice of auxiliary ligands is unusual. Tuning interligand electronic interactions and excited-state symmetry provides a new perspective for designing more efficient molecular and nanomaterials for photochemical and photophysical applications.

EXPERIMENTAL SECTION

General Methods. The dimolybdenum compounds are air and moisture sensitive. Syntheses and handling of metal compounds and ligands were conducted using standard Schlenk line and glovebox techniques. All of the solvents used were thoroughly dried and degassed. The homoleptic carboxylate precursor compounds were prepared from $Mo(CO)_6$ with established methods.[17,20] Details of the preparation of **I**−**IV** through exchange reactions are included in the Supporting Information.

NMR spectra of **I**−**IV** were recorded on a 400 MHz Bruker DPX Advance 400 spectrometer. All ^{1}H NMR chemical shifts are in ppm relative to the protio impurity in chloroform-*d* at 7.26 ppm. Matrix-assisted laser desorption ionization time-of-flight (MALDI-TOF) mass spectra were obtained on a Bruker Microflex mass spectrometer. Dithranol was used as the matrix. Nine peptides with molecular masses ranging from 450 to 3100 Da were used for calibration.

Crystal Structure Determination. Suitable crystals of **I**, **II**, and **IV** for X-ray crystallography were grown by the diffusion of hexanes into concentrated THF solutions of **I**, **II**, and **IV** containing a small amount of DMSO. Diffraction data were collected on a Nonius Kappa Apex II CCD diffractometer with Mo Kα radiation. All work was done at 150 K using an Oxford Cryosystems Cryostream Cooler.

Photophysical Measurements. UV−vis absorption and emission spectra of **I**−**IV** were collected under air-free conditions using a 1 cm × 1 cm quartz cell equipped with a Kontes stopcock. The absorption data were recorded on a PerkinElmer Lambda 900 spectrometer, and the emission data were recorded on a SPEX Fluoromax-2 fluorometer. $Ru(bpy)_3(PF_6)_2$ was used as a standard in the quantum-yield determination. FT-IR spectra of **I**−**IV** were collected on a PerkinElmer Spectrum GX FTIR spectrometer. Sample solutions were sealed in a PerkinElmer semidemountable cell with CaF_2 windows and a 0.1 mm Teflon spacer.

Femtosecond time-resolved infrared (fs-TRIR) experiments were performed using a Ti:sapphire oscillator/regenerative amplifier combination (1 kHz, fwhm ∼200 fs), as previously described.[40] The mid-IR probe/reference beams were generated through a difference

DOI: 10.1021/acs.inorgchem.7b01164
Inorg. Chem. XXXX, XXX, XXX−XXX

frequency generation (DFG) mechanism and was collected with a Triax 320 spectrometer, where they were dispersed with a grating onto separate arrays of a liquid nitrogen-cooled HgCdTe detector (32 × 2 pixels). Samples of **I**–**IV** were prepared to have ∼1 absorption at their MLCT peaks. Sample solutions were kept air-free in a PerkinElmer semidemountable cell with a 0.1 mm Teflon spacer and two 4.0 mm CaF_2 windows. The excitation-beam power at the sample was tuned to 1–2 μJ.

All time-resolved spectra were plotted in Igor Pro 6.0. Kinetic traces were fitted with a global fitting package with a sum of exponentials, $S(t) = \Sigma_i A_i \exp(-1/\tau_i) + C$, where A_i is the amplitude, τ_i is the lifetime, and C is an offset.

Computational Methods. Compounds **I**–**IV** were studied using density functional theory (DFT) methods with the B3LYP functional in the Gaussian09D01 suite. The 6-31G(d) basis set was used for the H, C, N, O, and F atoms, and the Stuttgart–Dresden (SDD) effective core potentials were used for Mo atoms.[41] Atomic coordinates from crystal structures were used as the initial input for structure optimization. Force constant and vibrational frequency analyses were performed on each compound to make sure that all structures are optimized to a global minimum. Isosurface contour plots of **I**–**IV** were created with Gaussview 5.0.8 with isovalues at 0.02. NBO 3.1 was used for the analysis of molecular orbital composition.[26] The polarizable continuum model (PCM) was used to account for the solvent effects, and default parameters were used for all the solvents.[42] A summary of solvent polarity moments, HOMO/LUMO energy levels and calculated MLCT wavelengths of **III** are presented in Figure S4 and Table S3 in the Supporting Information.

The vibration frequency analyses of **I**–**IV** were performed and used in the FT-IR spectra interpretation. All frequencies were scaled by a factor of 0.961 as suggested.[43]

■ ASSOCIATED CONTENT

Supporting Information

The Supporting Information is available free of charge on the ACS Publications website at DOI: 10.1021/acs.inorgchem.7b01164.

Crystal structure refinement information on **I**, **II**, and **IV**, NBO analysis, NMR, and MALDI-TOF spectra of **I**–**IV** (PDF)

Accession Codes

CCDC 1541002–1541003 and 1541005 contain the supplementary crystallographic data for this paper. These data can be obtained free of charge via www.ccdc.cam.ac.uk/data_request/cif, by emailing data_request@ccdc.cam.ac.uk, or by contacting The Cambridge Crystallographic Data Centre, 12 Union Road, Cambridge CB2 1EZ, UK; fax: +44 1223 336033.

■ AUTHOR INFORMATION

Corresponding Author

*E-mail: jiang.627@osu.edu.

ORCID

Changcheng Jiang: 0000-0002-7674-6883

Notes

The authors declare no competing financial interest.

■ ACKNOWLEDGMENTS

We would like to thank the National Science Foundation for the funding associated with grant numbers CHE-0957191 and CHE-1266298. We thank Prof. Claudia Turro for valuable discussions. We are grateful to the Ohio State University Center for Chemical and Biophysical Dynamics for use of the laser systems and the Ohio Supercomputer Center for computational resources.

■ REFERENCES

(1) Chergui, M. On the Interplay between Charge, Spin and Structural Dynamics in Transition Metal Complexes. *Dalton Trans.* **2012**, *41*, 13022.

(2) Zhang, W.; Gaffney, K. J. Mechanistic Studies of Photoinduced Spin Crossover and Electron Transfer in Inorganic Complexes. *Acc. Chem. Res.* **2015**, *48*, 1140–1148.

(3) Lomont, J. P.; Nguyen, S. C.; Harris, C. B. Ultrafast Infrared Studies of the Role of Spin States in Organometallic Reaction Dynamics. *Acc. Chem. Res.* **2014**, *47*, 1634–1642.

(4) Prier, C. K.; Rankic, D. A.; MacMillan, D. W. C. Visible Light Photoredox Catalysis with Transition Metal Complexes: Applications in Organic Synthesis. *Chem. Rev.* **2013**, *113*, 5322–5363.

(5) Arias-Rotondo, D. M.; McCusker, J. K. The Photophysics of Photoredox Catalysis: A Roadmap for Catalyst Design. *Chem. Soc. Rev.* **2016**, *45*, 5803–5820.

(6) Yeh, A. T.; Shank, C. V.; McCusker, J. K. Ultrafast Electron Localization Dynamics Following Photo-Induced Charge Transfer. *Science* **2000**, *289*, 935–938.

(7) Stark, C. W.; Schreier, W. J.; Lucon, J.; Edwards, E.; Douglas, T.; Kohler, B. Interligand Electron Transfer in Heteroleptic Ruthenium(II) Complexes Occurs on Multiple Time Scales. *J. Phys. Chem. A* **2015**, *119*, 4813–4824.

(8) Beljonne, D.; Wittmann, H. F.; Köhler, A.; Graham, S.; Younus, M.; Lewis, J.; Raithby, P. R.; Khan, M. S.; Friend, R. H.; Brédas, J. L. Spatial Extent of the Singlet and Triplet Excitons in Transition Metal-containing Poly-ynes. *J. Chem. Phys.* **1996**, *105*, 3868–3877.

(9) Silverman, L. N.; Kanchanawong, P.; Treynor, T. P.; Boxer, S. G. Stark Spectroscopy of Mixed-Valence Systems. *Philos. Trans. R. Soc., A* **2008**, *366*, 33–45.

(10) Dattelbaum, D. M.; Omberg, K. M.; Schoonover, J. R.; Martin, R. L.; Meyer, T. J. Application of Time-Resolved Infrared Spectroscopy to Electronic Structure in Metal-to-Ligand Charge-Transfer Excited States. *Inorg. Chem.* **2002**, *41*, 6071–6079.

(11) Alberding, B. G.; Chisholm, M. H.; Gallucci, J. C.; Ghosh, Y.; Gustafson, T. L. Electron Delocalization in the S_1 and T_1 Metal-to-Ligand Charge Transfer States of Trans-Substituted Metal Quadruply Bonded Complexes. *Proc. Natl. Acad. Sci. U. S. A.* **2011**, *108*, 8152–8156.

(12) Chisholm, M. H.; Lear, B. J. M2δ to Ligand π-Conjugation: Testbeds for Current Theories of Mixed Valence in Ground and Photoexcited States of Molecular Systems. *Chem. Soc. Rev.* **2011**, *40*, 5254.

(13) Chisholm, M. H. Charge Distribution in Metal to Ligand Charge Transfer States of Quadruply Bonded Metal Complexes. *Coord. Chem. Rev.* **2015**, *282–283*, 60–65.

(14) Chisholm, M. H.; Brown-Xu, S. E.; Spilker, T. F. Photophysical Studies of Metal to Ligand Charge Transfer Involving Quadruply Bonded Complexes of Molybdenum and Tungsten. *Acc. Chem. Res.* **2015**, *48*, 877–885.

(15) Jiang, C.; Young, P. J.; Durr, C. B.; Spilker, T. F.; Chisholm, M. H. Synthesis, Structure, and Photophysical Properties of $Mo_2(NN)_4$ and $Mo_2(NN)_2(T^iPB)_2$, Where NN = *N*, *N* ′-Diphenylphenylpropiolamidinate and T^iPB = 2,4,6-Triisopropylbenzoate. *Inorg. Chem.* **2016**, *55*, 5836–5844.

(16) Jiang, C.; Young, P. J.; Brown-Xu, S.; Gallucci, J. C.; Chisholm, M. H. Femtosecond Study of Dimolybdenum Paddlewheel Compounds with Amide/Thioamide Ligands: Symmetry, Electronic Structure, and Charge Distribution in the ^{1}MLCT S_1 State. *Inorg. Chem.* **2017**, *56*, 1433–1445.

(17) Brown, D. J.; Chisholm, M. H.; Gallucci, J. C. Amidinate–carboxylate Complexes of Dimolybdenum and Ditungsten: $M_2(O_2CR)_2((N^iPr)_2CR')_2$. Preparations, Molecular and Electronic Structures and Reactions. *Dalton Trans.* **2008**, No. 12, 1615.

(18) Alberding, B. G.; Brown-Xu, S. E.; Chisholm, M. H.; Gustafson, T. L.; Reed, C. R.; Naseri, V. Photophysical Properties of MM Quadruply Bonded Complexes (M = Mo, W) Supported by Carboxylate Ligands: Charge Delocalization and Dynamics in S_1 and T_1 States. *Dalton Trans.* **2012**, *41*, 13097.

DOI: 10.1021/acs.inorgchem.7b01164
Inorg. Chem. XXXX, XXX, XXX–XXX

(19) Hicks, J.; Ring, S. P.; Patmore, N. J. Tuning the Electronic Structure of Mo−Mo Quadruple Bonds by N for O for S Substitution. *Dalton Trans.* **2012**, *41*, 6641.
(20) *Multiple Bonds between Metal Atoms*, 3rd ed.; Cotton, F. A., Murillo, C. A., Walton, R. A., Eds.; Springer Science and Business Media: New York, NY, 2005.
(21) Cotton, F. A.; Norman, J. G. Molybdenum(II) Trifluoroacetate Dimer. Bispyridine Adduct. *J. Am. Chem. Soc.* **1972**, *94*, 5697−5702.
(22) Brown-Xu, S. E.; Chisholm, M. H.; Durr, C. B.; Spilker, T. F. Concerning the Ground State and S_1 and T_1 Photoexcited States of the Homoleptic Quadruply Bonded Complexes $Mo_2(O_2CC_6H_4\text{-}P\text{-}X)_4$, Where X = C≡C−H or C≡N. *J. Phys. Chem. A* **2013**, *117*, 13893−13898.
(23) Frisch, M. J.; Trucks, G. W.; Schlegel, H. B.; Scuseria, G. E.; Robb, M. A.; Cheeseman, J. R.; Scalmani, G.; Barone, V.; Mennucci, B.; Petersson, G. A.; Nakatsuji, H.; Caricato, M.; Li, X.; Hratchian, H. P.; Izmaylov, A. F.; Bloino, J.; Zheng, G.; Sonnenberg, J. L.; Hada, M.; Ehara, M.; Toyota, K.; Fukuda, R.; Hasegawa, J.; Ishida, M.; Nakajima, T.; Honda, Y.; Kitao, O.; Nakai, H.; Vreven, T.; Montgomery, J. A., Jr.; Peralta, J. E.; Ogliaro, F.; Bearpark, M.; Heyd, J. J.; Brothers, E.; Kudin, K. N.; Staroverov, V. N.; Kobayashi, R.; Normand, J.; Raghavachari, K.; Rendell, A.; Burant, J. C.; Iyengar, S. S.; Tomasi, J.; Cossi, M.; Rega, N.; Millam, J. M.; Klene, M.; Knox, J. E.; Cross, J. B.; Bakken, V.; Adamo, C.; Jaramillo, J.; Gomperts, R.; Stratmann, R. E.; Yazyev, O.; Austin, A. J.; Cammi, R.; Pomelli, C.; Ochterski, J. W.; Martin, R. L.; Morokuma, K.; Zakrzewski, V. G.; Voth, G. A.; Salvador, P.; Dannenberg, J. J.; Dapprich, S.; Daniels, A. D.; Farkas, O.; Foresman, J. B.; Ortiz, J. V.; Cioslowski, J.; Fox, D. J. *Gaussian 09*, revision D.01; Gaussian, Inc.: Wallingford, CT, 2009.
(24) Becke, A. D. Density-Functional Exchange-Energy Approximation with Correct Asymptotic Behavior. *Phys. Rev. A: At., Mol., Opt. Phys.* **1988**, *38*, 3098−3100.
(25) Alberding, B. G.; Chisholm, M. H.; Gustafson, T. L. Detection of the Singlet and Triplet MM $\Delta\delta^*$ States in Quadruply Bonded Dimetal Tetracarboxylates (M = Mo, W) by Time-Resolved Infrared Spectroscopy. *Inorg. Chem.* **2012**, *51*, 491−498.
(26) Glendening, E. D.; Reed, A. E.; Carpenter, J. E.; Weinhold, F. *NBO Version 3.1*; Theoretical Chemistry Institute: Madison, Wisconsin.
(27) Lu, T.; Chen, F. Multiwfn: A Multifunctional Wavefunction Analyzer. *J. Comput. Chem.* **2012**, *33*, 580−592.
(28) Terenziani, F.; Painelli, A.; Katan, C.; Charlot, M.; Blanchard-Desce, M. Charge Instability in Quadrupolar Chromophores: Symmetry Breaking and Solvatochromism. *J. Am. Chem. Soc.* **2006**, *128*, 15742−15755.
(29) Demadis, K. D.; Hartshorn, C. M.; Meyer, T. J. The Localized-to-Delocalized Transition in Mixed-Valence Chemistry. *Chem. Rev.* **2001**, *101*, 2655−2686.
(30) Brown-Xu, S. E.; Chisholm, M. H.; Durr, C. B.; Lewis, S. A.; Spilker, T. F.; Young, P. J. Mo_2 Paddlewheel Complexes Functionalized with a Single MLCT, S_1 Infrared-Active Carboxylate Reporter Ligand: Preparation and Studies of Ground and Photoexcited States. *Inorg. Chem.* **2014**, *53*, 637−644.
(31) Lear, B. J.; Glover, S. D.; Salsman, J. C.; Londergan, C. H.; Kubiak, C. P. Solvent Dynamical Control of Ultrafast Ground State Electron Transfer: Implications for Class II−III Mixed Valency. *J. Am. Chem. Soc.* **2007**, *129*, 12772−12779.
(32) Li, C.; Hoffman, M. Z. Electron Localization or Delocalization in the MLCT Excited States of $Ru(bpy)_3^{2+}$ and $Ru(phen)_3^{2+}$. Consequences to Their Photochemistry and Photophysics in Fluid Solution. *Inorg. Chem.* **1998**, *37*, 830−832.
(33) El Nahhas, A.; Consani, C.; Blanco-Rodríguez, A. M.; Lancaster, K. M.; Braem, O.; Cannizzo, A.; Towrie, M.; Clark, I. P.; Záliš, S.; Chergui, M.; et al. Ultrafast Excited-State Dynamics of Rhenium(I) Photosensitizers $[Re(Cl)(CO)_3(N,N)]$ and $[Re(imidazole)(CO)_3(N,N)]^+$: Diimine Effects. *Inorg. Chem.* **2011**, *50*, 2932−2943.
(34) Auböck, G.; Chergui, M. Sub-50-Fs Photoinduced Spin Crossover in $[Fe(bpy)_3]^{2+}$. *Nat. Chem.* **2015**, *7*, 629−633.
(35) Cooper, T. M.; Krein, D. M.; Burke, A. R.; McLean, D. G.; Rogers, J. E.; Slagle, J. E.; Fleitz, P. A. Spectroscopic Characterization of a Series of Platinum Acetylide Complexes Having a Localized Triplet Exciton. *J. Phys. Chem. A* **2006**, *110*, 4369−4375.
(36) Cooper, T. M.; Krein, D. M.; Burke, A. R.; McLean, D. G.; Rogers, J. E.; Slagle, J. E. Asymmetry in Platinum Acetylide Complexes: Confinement of the Triplet Exciton to the Lowest Energy Ligand. *J. Phys. Chem. A* **2006**, *110*, 13370−13378.
(37) Liu, Y.; Jiang, S.; Glusac, K.; Powell, D. H.; Anderson, D. F.; Schanze, K. S. Photophysics of Monodisperse Platinum-Acetylide Oligomers: Delocalization in the Singlet and Triplet Excited States. *J. Am. Chem. Soc.* **2002**, *124*, 12412−12413.
(38) Wilson, J. S.; Wilson, R. J.; Friend, R. H.; Köhler, A.; Al-Suti, M. K.; Al-Mandhary, M. R. A.; Khan, M. S. Polarization of Singlet and Triplet Excited States in a Platinum-Containing Conjugated Polymer. *Phys. Rev. B: Condens. Matter Mater. Phys.* **2003**, *67*, 125206.
(39) Dereka, B.; Rosspeintner, A.; Krzeszewski, M.; Gryko, D. T.; Vauthey, E. Symmetry-Breaking Charge Transfer and Hydrogen Bonding: Toward Asymmetrical Photochemistry. *Angew. Chem., Int. Ed.* **2016**, *55*, 15624−15628.
(40) Wang, J.; Burdzinski, G.; Kubicki, J.; Platz, M. S. Ultrafast UV−Vis and IR Studies of *P*-Biphenylyl Acetyl and Carbomethoxy Carbenes. *J. Am. Chem. Soc.* **2008**, *130*, 11195−11209.
(41) Andrae, D.; Häußermann, U.; Dolg, M.; Stoll, H.; Preuß, H. Energy-Adjustedab Initio Pseudopotentials for the Second and Third Row Transition Elements. *Theor. Chim. Acta* **1990**, *77*, 123−141.
(42) Cossi, M.; Scalmani, G.; Rega, N.; Barone, V. New Developments in the Polarizable Continuum Model for Quantum Mechanical and Classical Calculations on Molecules in Solution. *J. Chem. Phys.* **2002**, *117*, 43−54.
(43) Irikura, K. K.; Johnson, R. D.; Kacker, R. N. Uncertainties in Scaling Factors for Ab Initio Vibrational Frequencies. *J. Phys. Chem. A* **2005**, *109*, 8430−8437.

DOI: 10.1021/acs.inorgchem.7b01164
Inorg. Chem. XXXX, XXX, XXX−XXX